

## Static and Dynamic Magnetism in Underdoped Superconductor $\text{BaFe}_{1.92}\text{Co}_{0.08}\text{As}_2$

A. D. Christianson, M. D. Lumsden, S. E. Nagler, G. J. MacDougall, M. A. McGuire, A. S. Sefat,  
R. Jin, B. C. Sales, and D. Mandrus

*Oak Ridge National Laboratory, Oak Ridge, Tennessee 37831, USA*

(Received 5 April 2009; published 19 August 2009)

We report neutron scattering measurements on single crystals of  $\text{BaFe}_{1.92}\text{Co}_{0.08}\text{As}_2$ . The magnetic Bragg peak intensity is reduced by 6% upon cooling through  $T_C$ . The spin dynamics exhibit a gap of 8 meV with anisotropic three-dimensional interactions. Below  $T_C$  additional intensity appears at an energy of  $\sim 4.5(0.5)$  meV, similar to previous observations of a spin resonance in other Fe-based superconductors. No further gapping of the spin excitations is observed below  $T_C$  for energies down to 2 meV. These observations suggest the redistribution of spectral weight from the magnetic Bragg position to a spin resonance, demonstrating the direct competition between static magnetic order and superconductivity.

DOI: 10.1103/PhysRevLett.103.087002

PACS numbers: 74.70.-b, 74.20.Mn, 78.70.Nx

Despite intense experimental and theoretical efforts directed towards understanding the recently discovered Fe-based superconductors [1–7], the mechanism behind superconductivity remains unclear (e.g., [8–13]). However, one common feature is the presence of magnetism in large regions of the phase diagrams for these materials (e.g., [14–17]). As such, there have been many suggestions that the pairing mechanism originates from spin fluctuations. The observation of a resonance, strongly coupled to  $T_C$ , in the spin dynamics of  $\text{BaFe}_2\text{As}_2$  doped with potassium [18], cobalt [19], and nickel [20] supports this contention and emphasizes the need for a comprehensive understanding of the fundamental magnetic behavior of these materials.

Consequently, numerous studies have been initiated to probe the magnetic behavior of the Fe-based superconductors. In  $A\text{Fe}_2\text{As}_2$  ( $A = \text{Ba}, \text{Sr}, \text{Ca}$ ), studies of the static magnetic properties have revealed spin density wave order with magnetic moments aligned along the  $a$  axis of the low temperature orthorhombic structure [17]. The spin excitations of these compounds are the subject of intense scrutiny as means of establishing the degree to which the magnetic behavior originates from localized or itinerant Fe  $3d$  electrons [17]. As noted above, the spin dynamics in superconducting samples have been studied in several members of optimally doped  $\text{BaFe}_2\text{As}_2$  [18–20] where both the tetragonal-orthorhombic structural distortion and long-range magnetic order have been suppressed. In particular, for doping levels where static magnetism coexists with superconductivity (either microscopically or as separate phases), the nature of the magnetic excitations has yet to be established in detail.

$\text{BaFe}_{2-x}\text{Co}_x\text{As}_2$  [21] has emerged as one of the most important systems in large part due to the availability of large homogenous single crystals. The phase diagram [22–24] for these materials shows that in the underdoped regime there is both a structural phase transition and a magnetic ordering transition, as in the parent compound.

For the range of concentrations,  $0.06 < x < 0.12$ , samples exhibit both magnetic order and superconductivity. The topic of this Letter is a neutron scattering study of single crystal samples of underdoped  $\text{BaFe}_{1.92}\text{Co}_{0.08}\text{As}_2$  with  $T_N = 58$  K and  $T_C = 11$  K. We observe a 6% reduction of the magnetic Bragg peak intensity on cooling through  $T_C$ . The reduction in intensity is not due to a change in the magnetic structure and hence represents either a reduction in the ordered moment or a decrease in the fraction of the sample exhibiting long-range magnetic order. On the other hand, the spin dynamics associated with the magnetic ordering is gapped above  $T_C$ , while below  $T_C$  additional intensity appears at an energy of  $\sim 4.5(0.5)$  meV consistent with the observation of a spin resonance in other Fe-based superconductors. Thus, a loss in spectral weight in the magnetic Bragg peaks appears to be compensated by the appearance of a spin resonance highlighting the competition between magnetic order and superconductivity. The intensity of the resonance observed for  $x = 0.08$  depends on  $\mathbf{Q}$  both in-plane and along the  $c$  axis in stark contrast to the two-dimensional resonance observed in the optimally doped sample [19]. We note that the neutron scattering data presented here do not allow for differentiation between microscopic coexistence and phase separation of superconductivity and magnetism.

Single crystals of  $\text{BaFe}_{1.92}\text{Co}_{0.08}\text{As}_2$  were grown using FeAs flux as described in [19]. Magnetic susceptibility and specific heat measurements on pieces from the same batches as the neutron scattering crystals yield  $T_C = 11$  K. Although at low temperature the crystal structure is strictly orthorhombic [22,24], the measurements reported here have insufficient resolution to observe the consequences of the structural distortion. For this reason and for consistency with previous inelastic measurements on superconducting samples [18,19], we use tetragonal notation exclusively. For reference (1 0  $L$ ), the antiferromagnetic ordering wave vector in orthorhombic notation is indexed as  $(\frac{1}{2} \frac{1}{2} L)$  in tetragonal notation.

Neutron diffraction data were collected on a 0.2 g crystal. For the inelastic neutron scattering measurements, four single crystals of  $\text{BaFe}_{1.92}\text{Co}_{0.08}\text{As}_2$  with a total mass of 2 g were coaligned with a mosaic of  $\sim 1^\circ$  in the  $(HLL)$  plane. The data in Fig. 1(b) were collected using the HB1A triple-axis spectrometer at the High Flux Isotope Reactor configured with collimations of  $48'-40'-40'-136'$ . The remainder of the data presented here were collected with the HB-3 triple-axis spectrometer at the High Flux Isotope Reactor configured with collimations of  $48'-60'-80'-120'$  with a fixed final energy of 14.7 meV using pyrolytic graphite monochromator and analyzer crystals.

Figure 1 shows neutron diffraction data as a function of temperature for  $\text{BaFe}_{1.92}\text{Co}_{0.08}\text{As}_2$ . Figure 1(a) shows the temperature dependence of the  $(\frac{1}{2} \frac{1}{2} 3)$  magnetic Bragg peak. Fits to a power law over a limited range of temperatures ( $30 \text{ K} < T < 80 \text{ K}$ ) yield an ordering temperature,  $T_N = 58(0.6) \text{ K}$ . Figure 1(b) indicates a significant reduction in intensity below  $T_C$  for both  $(\frac{1}{2} \frac{1}{2} 1)$  and  $(\frac{1}{2} \frac{1}{2} 3)$ . The intensity at 1.6 K is reduced by 6% relative to that of the maximum intensity found at  $T_C$ . The change in intensity of both peaks occurs in the same manner so that the effect cannot be explained by a change in magnetic structure or a spin reorientation. Transverse and longitudinal scans were made through  $(\frac{1}{2} \frac{1}{2} 1)$  and  $(\frac{1}{2} \frac{1}{2} 3)$  to ensure that the observed change is due to a reduction in the integrated intensity rather than a change in peak position or line width. The full width at half maximum (FWHM) and peak positions extracted from fits to the  $(\frac{1}{2} \frac{1}{2} 3)$  peak are shown in Figs. 1(c) and 1(d). A Gaussian line shape was

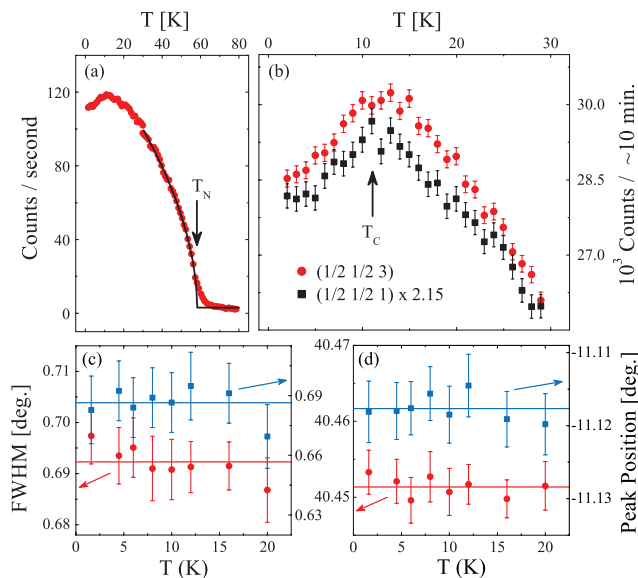


FIG. 1 (color). (a) Peak intensity of the  $(\frac{1}{2} \frac{1}{2} 3)$  magnetic Bragg peak. The solid line is the result of a power law fit as described in the text. (b) Peak intensity of the  $(\frac{1}{2} \frac{1}{2} 1)$  and  $(\frac{1}{2} \frac{1}{2} 3)$  magnetic peaks through  $T_C$ . The FWHM (c) and peak position (d) extracted from transverse and longitudinal scans in terms of  $\theta$  (squares) and  $2\theta$  (circles) for the  $(\frac{1}{2} \frac{1}{2} 3)$  peak through  $T_C$ . The solid lines in (c) and (d) represent the weighted average.

used for the longitudinal and a Lorentzian squared line shape was used for the transverse scans. Together these graphs show neither the FWHM (resolution limited) nor the peak position changes significantly through  $T_C$ . The background extracted from fits to the peak position and FWHM as well as measurements at  $(\frac{1}{2} \frac{1}{2} 2.7)$  (not shown) indicate no change in the background through  $T_C$ . Thus, there is either a reduction in the ordered magnetic moment or a reduction in the fraction of the sample that is magnetically ordered that is coincident with the onset of superconductivity in  $\text{BaFe}_{1.92}\text{Co}_{0.08}\text{As}_2$ . A somewhat larger reduction in magnetic Bragg peak intensity has also been seen by Pratt *et al.* [22] for a sample with a slightly higher Co doping and consequently a higher  $T_C$  and lower  $T_N$ . Together these results show that competition between magnetism and superconductivity is robust in the underdoped region of these materials in samples with different  $T_C$  and synthesized by different groups.

Naturally the question arises, What happens to the spectral weight associated with the reduced Bragg peak intensity below  $T_C$ ? As we discuss below, the spin excitations may provide the answer. Figure 2(a) shows a constant- $Q$  scan at the  $(\frac{1}{2} \frac{1}{2} \bar{1})$  wave vector at 1.6 ( $T < T_C$ ) and 20 K ( $T > T_C$ ). For comparison, we show the background esti-

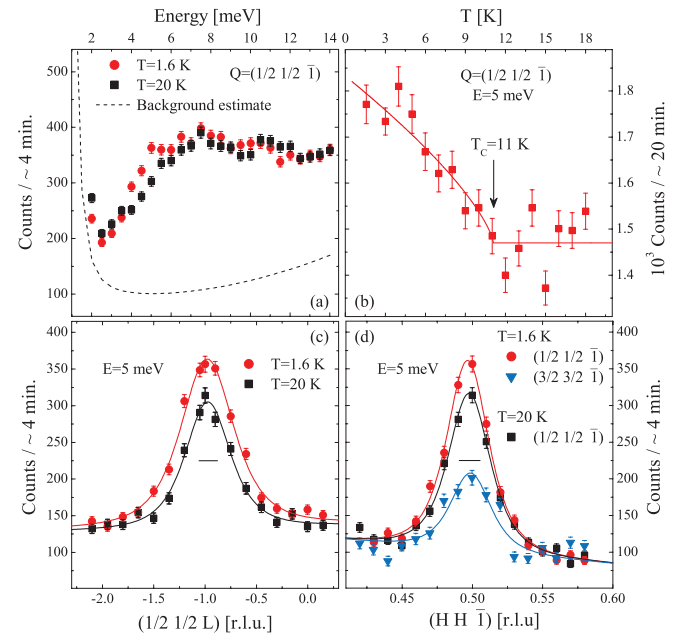


FIG. 2 (color). (a) Constant- $Q$  scans,  $Q = (\frac{1}{2} \frac{1}{2} \bar{1})$ , for temperatures above and below  $T_C$ . For comparison the background scattering determined as described in the text is also shown. (b) The temperature dependence of the inelastic intensity at  $(\frac{1}{2} \frac{1}{2} \bar{1})$  and  $E = 5 \text{ meV}$ . The solid line is a power law fit yielding  $T_C = 11(1) \text{ K}$ .  $L$  dependence (c) and  $H$  dependence (d) of the inelastic intensity near  $Q = (\frac{1}{2} \frac{1}{2} \bar{1})$  and  $E = 5 \text{ meV}$  at 1.6 and 20 K. The solid lines are guides to the eye, and the horizontal bars represent instrumental resolution. The unit r.l.u. denotes reciprocal lattice units. In (d) a scan around  $(\frac{3}{2} \frac{3}{2} \bar{1})$  is included to emphasize the magnetic origin of the scattering.

mated from combining constant- $E$  scans with the constant- $Q$  scan at  $(0.65, 0.65, \bar{1})$ . This scattering has only negligible temperature dependence. The data at 1.6 K show additional intensity at an energy of  $\sim 5$  meV. Figures 2(c) and 2(d) show the in-plane and out-of-plane wave vector dependence of the spin excitations above and below  $T_C$  near  $(\frac{1}{2}, \frac{1}{2}, \bar{1})$ . Unlike optimally doped samples [19] the intensity is strongly peaked both in-plane and out-of-plane, indicating three-dimensional (3D) spin correlations. Figure 2(b) shows the evolution of the extra intensity as a function of temperature. A power law fit yields a  $T_C$  of 11 (1) K in agreement with the bulk measurements on these samples, demonstrating a strong coupling between the appearance of the resonance and superconductivity.

In the optimally doped samples, the intensity gained at the resonance energy for  $T < T_C$  is compensated by the opening of a spin gap at lower energy [18–20]. To search for such a gap in this case, thermal population effects must be removed. To this end, the dynamic susceptibility  $[\chi''(\mathbf{Q}, \omega)]$  has been derived from the data in Fig. 2(a) by removing the background scattering, correcting for thermal population, and applying a correction for higher order contamination in the beam monitor. The resulting  $\chi''(\mathbf{Q}, \omega)$  at 1.6 and 20 K is shown in Fig. 3(a). This shows that a spin gap is already present at 20 K and that an additional gap does not open below  $T_C$  for energies as low as 2 meV. In this case, a likely origin for the additional spectral weight required for the change in  $\chi''(\mathbf{Q}, \omega)$  is the loss of spectral weight at the magnetic Bragg peak positions. A full confirmation of this contention requires a complete measurement of the magnetic scattering across an entire Brillouin zone. These data appear to be in contrast

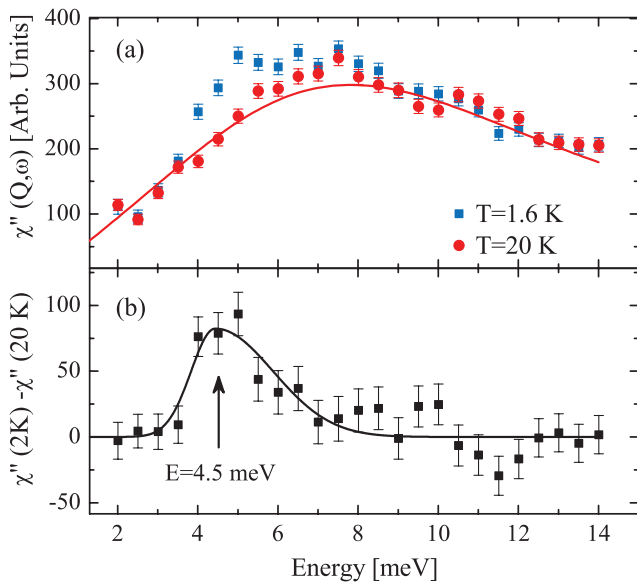


FIG. 3 (color). (a)  $\chi''(\mathbf{Q}, \omega)$  for  $\mathbf{Q} = (\frac{1}{2}, \frac{1}{2}, \bar{1})$  at 1.6 and 20 K. The line is a fit to  $\chi''$  at 20 K as described in the text. (b) The difference between  $\chi''(\mathbf{Q}, \omega)$  at 1.6 and 20 K showing an additional component to the spin dynamics which appears below  $T_C$ . The line is a guide to the eye.

to the conclusions of [22] which claim gapless spin excitations below  $T_N$  with a gap opening below  $T_C$ . We note that our measurements extend over a wider energy range and were performed with fixed  $E_f$ . For the constant  $E_i$  data presented in [22], an additional correction for resolution volume [25] is required to extract  $\chi''(\mathbf{Q}, \omega)$ . In fact, we can transform our measured  $\chi''(\mathbf{Q}, \omega)$  to provide an estimate of the quantity measured with fixed  $E_i$ . Doing so yields a neutron scattering intensity nearly identical to that of [22], indicating no inconsistency between the two data sets.

Figure 3(b) shows the difference between the dynamic susceptibility,  $\chi''(\mathbf{Q} = (\frac{1}{2}, \frac{1}{2}, \bar{1}), \omega)$ , at 1.6 and 20 K. This emphasizes the appearance of the resonant intensity below  $T_C$  with a maximum at  $E = 4.5(0.5)$  meV or  $4.7k_B T_C$ . This is consistent with the energy of the spin resonance observed for other Fe-based superconductors [18–20], indicating universality across the phase diagram. In contrast to the data reported for an optimally Co-doped sample [19], the spin resonance intensity varies strongly with  $L$  and is only observed for  $L$  near the antiferromagnetic zone center as shown in Fig. 2(c).

To explore the spin excitations in more detail, a series of constant- $E$  scans along  $(H, H, \bar{1})$  and  $(\frac{1}{2}, \frac{1}{2}, L)$  are shown in Fig. 4. These measurements show data peaked in both  $H$  and  $L$  for energies up to 11 meV, indicating anisotropic 3D interactions as in the parent compound [26]. To quantitatively analyze the spin wave dispersion, we consider a Heisenberg model with in-plane near-neighbor coupling constants  $J_{1a}$  and  $J_{1b}$ , next near-neighbor coupling constant  $J_2$ , a  $c$  axis coupling constant  $J_c$ , and anisotropy  $D$  as described previously [26–28]. The dispersion for this Hamiltonian is  $\omega_q = \sqrt{A_q^2 - B_q^2}$  where  $A_q = 2S(\{J_{1b} \cos[\pi(H - K)] - 1\} + J_{1a} + J_c + 2J_2 + D)$ ,  $B_q = 2S(J_{1a} \cos[\pi(H + K)] + 2J_2 \cos\{\pi(H + K) \cos[\pi(H - K)]\} + J_c \cos(\pi L))$ . To analyze the data, we convolved the following  $S(\mathbf{Q}, \omega)$  (e.g., [29]) with the instrumental resolution function:

$$S(\mathbf{Q}, \omega) \propto \frac{A_q - B_q}{\omega_q} \frac{4}{\pi} \frac{\Gamma \omega \omega_q}{(\omega^2 - \omega_q^2)^2 + 4(\Gamma \omega)^2} \quad (1)$$

Fits were performed to constant- $E$  scans measured at 1.6 K except for  $E = 5$  meV where data taken from 20 K were analyzed to prevent the inclusion of resonance intensity. Excluding the 5 meV data from the fits does not significantly alter the results. The data were corrected for the Bose factor and the contamination of the beam monitor by higher order scattering from the monochromator. The model describes the data well with the inclusion of a large damping parameter,  $\Gamma = 6.2$  meV. Similar broad scattering was observed in measurements on  $\text{BaFe}_2\text{As}_2$  [26]. To properly describe a heavily damped spin excitation a damped harmonic oscillator, as opposed to a Lorentzian, is essential to prevent divergence of  $\chi''$  at small energies. The solid lines shown in Fig. 4 as well as the solid line through the 20 K constant- $Q$  scan in Fig. 3(a) are the

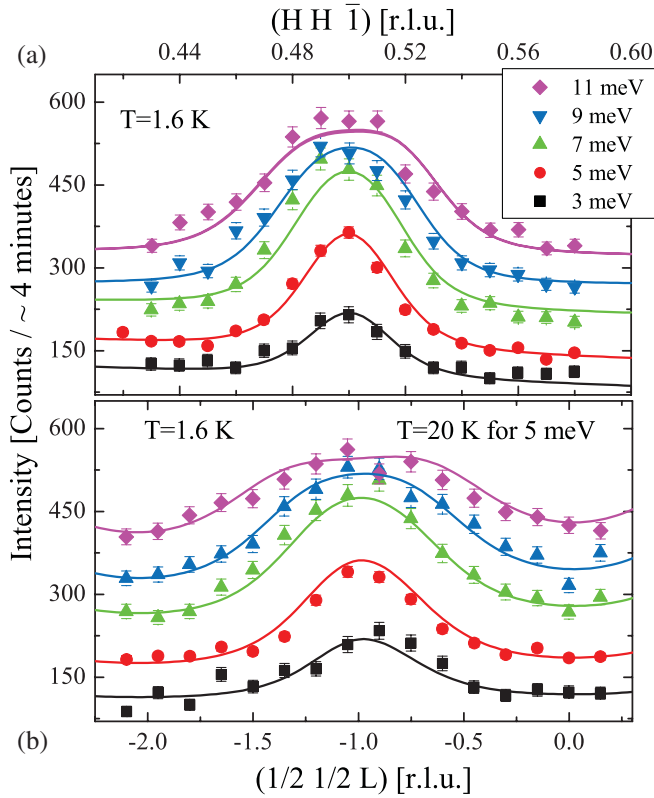


FIG. 4 (color). (a) Constant- $E$  scans along  $(H H \bar{1})$ . (b) Constant- $E$  scans along  $(\frac{1}{2} \frac{1}{2} L)$ . All data are measured at 1.6 K except  $E = 5$  meV, measured at 20 K to prevent the introduction of spin resonance scattering. The solid lines represent fits to the model with a single amplitude as described in the text. The scans are offset by 50 counts for clarity.

results of the fits with a common amplitude. Measurements in the  $(HHL)$  scattering plane at these energies are insensitive to  $J_{1b}$  and only depend on  $J_{1a}$  and  $J_2$  via  $J_{1a} + 2J_2$ . This was confirmed by considering multiple values of  $J_{1b}$  and ratios of  $J_{1a}/2J_2$ , all yielding identical results. The best fit values are  $S(J_{1a} + 2J_2) = 32.0(1)$  meV,  $SJ_c = 0.34(1)$  meV, and  $SD = 0.25(1)$  meV yielding a gap energy of 8.1(2) meV. The value of the gap energy is strongly affected by the choice of line shape, and hence, care must be taken when comparing to other parametrizations [26]. On the other hand, the spin wave velocities are not so strongly dependent on the line shape choice, and the best fit parameters yield velocities of  $v_{\parallel} = 180$  meV  $\text{\AA}$  and  $v_{\perp} = 43$  meV  $\text{\AA}$  and an anisotropy ratio of 4.2. This ratio is consistent with measurements on  $\text{BaFe}_2\text{As}_2$  [26], indicating little change in anisotropy. This is in contrast with the optimally doped measurements where the excitations were found to be much more two-dimensional [19]. This suggests that the presence of the structural phase transition may be responsible for the three dimensionality in these systems, a conclusion which is consistent with recent ARPES measurements [30].

In summary, neutron scattering measurements on single crystals of  $\text{BaFe}_{1.92}\text{Co}_{0.08}\text{As}_2$  indicate spin waves which

exhibit a gap of 8 meV and anisotropic 3D interactions. On cooling below  $T_C$ , a reduction in the magnetic Bragg peak intensity of 6% is observed with the simultaneous appearance of a resonance at the same wave vector with a characteristic energy of  $4.7k_B T_C$ . In addition, there is no evidence of an additional spin gap developing below  $T_C$ . Taken together these conclusions support a picture where spectral weight is transferred from ordered magnetic moments to spin fluctuations in  $\text{BaFe}_{1.92}\text{Co}_{0.08}\text{As}_2$ , in contrast to optimally doped samples [18–20] with no long-range magnetic order where a gap in the excitation spectrum opens contributing the spectral weight required to produce a resonance.

We acknowledge discussions with A. Zheludev, D. Singh, H. Mook, T. Egami, T. Maier, and D. Scalapino. This work was supported by the Scientific User Facilities Division and the Division of Materials Sciences and Engineering, Office of Basic Energy Sciences, DOE.

- 
- [1] Y. Kamihara *et al.*, *J. Am. Chem. Soc.* **130**, 3296 (2008).
  - [2] X. H. Chen *et al.*, *Nature (London)* **453**, 761 (2008).
  - [3] G. F. Chen *et al.*, *Phys. Rev. Lett.* **100**, 247002 (2008).
  - [4] Z.-A. Ren *et al.*, *Europhys. Lett.* **83**, 17002 (2008).
  - [5] M. Rotter, M. Tegel, and D. Johrendt, *Phys. Rev. Lett.* **101**, 107006 (2008).
  - [6] X. C. Wang *et al.*, *Solid State Commun.* **148**, 538 (2008).
  - [7] Kuo-Wei Yeh *et al.*, *Europhys. Lett.* **84**, 37002 (2008).
  - [8] A. V. Chubukov, arXiv:0902.4188.
  - [9] V. Cvetkovic *et al.*, *Europhys. Lett.* **85**, 37002 (2009).
  - [10] Y. Bang *et al.*, *Phys. Rev. B* **78**, 134523 (2008).
  - [11] W.-Q. Chen *et al.*, *Phys. Rev. Lett.* **102**, 047006 (2009).
  - [12] I. I. Mazin and J. Schmalian, arXiv:0901.4790.
  - [13] D. J. Singh and M. H. Du, *Phys. Rev. Lett.* **100**, 237003 (2008).
  - [14] C. de la Cruz *et al.*, *Nature (London)* **453**, 899 (2008).
  - [15] M. A. McGuire *et al.*, *Phys. Rev. B* **78**, 094517 (2008).
  - [16] Q. Huang *et al.*, *Phys. Rev. Lett.* **101**, 257003 (2008).
  - [17] J. W. Lynn and P. Dai, arXiv:0902.0091.
  - [18] A. D. Christianson *et al.*, *Nature (London)* **456**, 930 (2008).
  - [19] M. D. Lumsden *et al.*, *Phys. Rev. Lett.* **102**, 107005 (2009).
  - [20] S. Chi *et al.*, *Phys. Rev. Lett.* **102**, 107006 (2009).
  - [21] A. S. Sefat *et al.*, *Phys. Rev. Lett.* **101**, 117004 (2008).
  - [22] D. K. Pratt *et al.*, preceding Letter, *Phys. Rev. Lett.* **103**, 087001 (2009).
  - [23] F. Ning *et al.*, *J. Phys. Soc. Jpn.* **78**, 013711 (2009).
  - [24] J.-H. Chu *et al.*, arXiv:0811.2463.
  - [25] G. Shirane, S. M. Shapiro, and J. M. Tranquada, *Neutron Scattering with a Triple-Axis Spectrometer* (Cambridge University Press, Cambridge, England, 2002).
  - [26] K. Matan *et al.*, *Phys. Rev. B* **79**, 054526 (2009).
  - [27] R. A. Ewings *et al.*, *Phys. Rev. B* **78**, 220501(R) (2008).
  - [28] To account for the low temperature orthorhombic structure, two domains of equal population were included.
  - [29] J. Zhao *et al.*, arXiv:0903.2686.
  - [30] C. Liu *et al.*, arXiv:0903.4388.